

MuDG: Taming Multi-modal Diffusion with Gaussian Splatting for Urban Scene Reconstruction

Yingshuang Zou^{1,2*} Yikang Ding^{2*†} Chuanrui Zhang^{1,2} Jiazhe Guo^{1,2} Bohan Li^{2,4}
Xiaoyang Lyu⁵ Feiyang Tan³ Xiaojuan Qi⁵ Haoqian Wang^{1‡}

¹THU ²MEGVII ³Mach Drive ⁴SJTU ⁵HKU

<https://github.com/heiheishuang/MuDG>

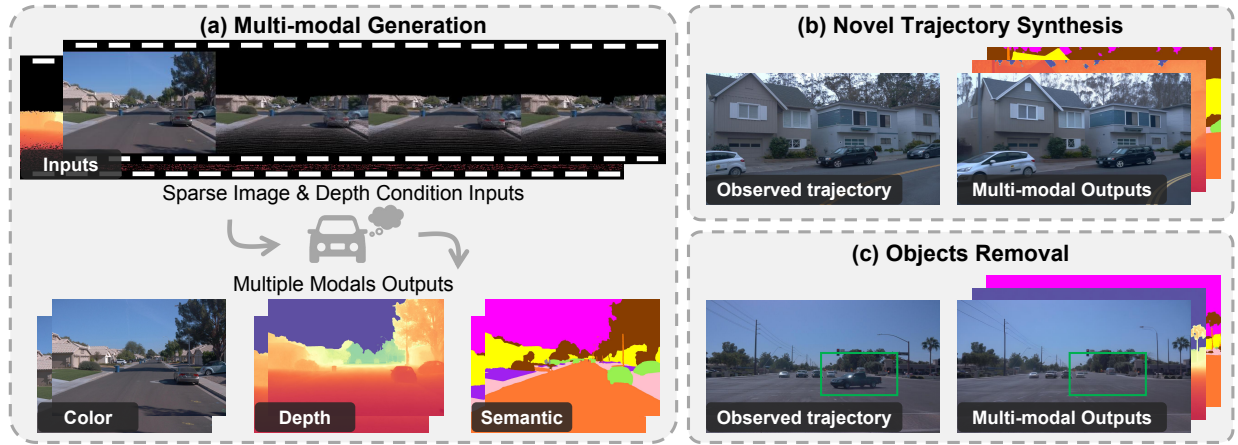


Figure 1. Given sparse sequential image-depth inputs, our multi-modal diffusion model enables controllable novel view synthesis, abstaining per-scene optimization. It also serves as a supervised signal to enhance the Gaussian Splatting model. Furthermore, its strong controllability allows for scene editing (e.g., object removal, background modification), providing valuable data for autonomous driving.

Abstract

Recent breakthroughs in radiance fields have significantly advanced 3D scene reconstruction and novel view synthesis (NVS) in autonomous driving. Nevertheless, critical limitations persist: reconstruction-based methods exhibit substantial performance deterioration under significant viewpoint deviations from training trajectories, while generation-based techniques struggle with temporal coherence and precise scene controllability. To overcome these challenges, we present **MuDG**, an innovative framework that integrates **M**ulti-modal **D**iffusion model with **G**aussian Splatting (GS) for Urban Scene Reconstruction. **MuDG** leverages aggregated LiDAR point clouds with RGB and geometric priors to condition a multi-modal video diffusion model, synthesizing photorealistic RGB, depth, and semantic outputs for novel viewpoints. This synthesis pipeline enables feed-forward NVS without computationally intensive per-scene optimization, providing comprehensive supervision signals to refine 3DGS representations for rendering

robustness enhancement under extreme viewpoint changes. Experiments on the Open Waymo Dataset demonstrate that MuDG outperforms existing methods in both reconstruction and synthesis quality.

1. Introduction

With the advancement of radiance field-based reconstruction techniques (e.g., NeRF [3, 21, 42], 3D Gaussian Splatting [11, 14, 40, 41]), 3D reconstruction and novel view synthesis (NVS) have been widely applied in AR/VR, robotics, and many other fields [4, 19]. In autonomous driving, such techniques enable dynamic urban scene reconstruction and view synthesis [2, 12, 33, 35, 38, 45, 47], offering a promising solution for synthetic data generation and closed-loop simulation. However, reconstructing and rendering high-fidelity sensor observations (RGB videos, LiDAR point clouds, and dense depth maps) remains challenging in complex driving environments.

To address this challenge, reconstruction-based approaches [2, 12, 33, 35, 37, 45, 46] extend NeRF and 3DGS to dynamic urban environments. These methods achieve

* Equal contribution. † Project Leader. ‡ Corresponding author.

scene decomposition by separating dynamic objects from static backgrounds via bbox tracking [33, 37, 45, 46] or self-supervised decomposition [2, 12, 35], demonstrating strong reconstruction quality and rendering performance along captured trajectories.

However, these reconstruction-centric methods still face limitations in NVS. When rendering viewpoints deviate significantly from the original trajectories, visual quality deteriorates rapidly, with severe artifacts emerging due to insufficient scene reconstruction. This fundamental limitation constrains their applicability in simulation scenarios requiring flexible viewpoint control. Meanwhile, emerging generation-based methods leverage diffusion models [7, 16, 29, 30, 39, 44] conditioned on control signals (*e.g.*, Bird’s-Eye-View (BEV) layouts and waypoints) for urban scene synthesis. While these generative approaches produce high-fidelity outputs, they struggle with consistency across multiple generations. The inherent stochasticity of diffusion processes introduces temporal incoherence and trajectory variation artifacts, which pose challenges for deployment in simulation systems and corner-case generation scenarios. We attribute the performance degradation of reconstruction-based methods under out-of-trajectory viewpoints to insufficient supervision during scene optimization, while the inconsistency in generative approaches arises from the lack of reliable and detailed conditions.

To address these challenges, we propose MuDG, a framework that integrates a controllable **M**ulti-modal **D**iffusion model with **G**aussian Splatting (GS) for Urban Scene Reconstruction. At its core, MuDG features a multi-modal video generation model conditioned on sparse point cloud projections, synthesizing RGB, depth, and semantic videos from novel viewpoints, as shown in Fig. 1. The generated results can serve not only as rendering outputs for novel views without requiring per-scene optimization but also as supervisory signals for training Gaussian Splatting models, enabling robust rendering under large viewpoint changes. Specifically, we aggregate LiDAR point clouds across multiple frames and separate dynamic and static elements using tracked bounding boxes. These point clouds retain RGB and geometry information from their original trajectories. For novel view synthesis, our model takes sparse RGB and depth from aggregated point cloud projections as input and generates dense results aligned with the projected viewpoints.

This multi-modal design leverages video generation priors to simulate GS rendering in a feed-forward manner, allowing direct application to novel scenes without per-scene optimization. Furthermore, the synthesized multi-model results provide rich supervision for subsequent GS training, which is important in reconstructing dynamic urban scenes, enabling the enhanced GS models to maintain high rendering quality even under substantial camera

movements. This effectively mitigates the performance degradation observed in conventional GS systems when extrapolating beyond training viewpoints. Our contributions are summarized as follows:

- A novel controllable multi-modal diffusion model for feed-forward synthesis of high-fidelity RGB, depth, and semantic segmentation outputs in novel view synthesis.
- Integration of multi-modal generation with Gaussian Splatting, achieving significant improvements in out-of-trajectory NVS quality for urban scenes.
- Extensive experiments on the Open Waymo Dataset (WOD) benchmark [23] indicate our approach outperforms existing methods.

2. Related Work

2.1. Novel View Synthesis for Urban Scene

Recent advancements in NeRF [3, 21, 25, 42] and 3D Gaussian Splatting (GS) [11, 14, 40] have driven progress in novel view synthesis for urban scenes [2, 12, 33, 35, 37, 45, 46], emphasizing real-time performance, spatial-temporal coherence, and controllability. Pioneering works like 3D Gaussian Splatting [13] achieve real-time radiance field rendering by optimizing anisotropic 3D Gaussians, enabling high-fidelity novel-view synthesis at 1080p resolution. To address dynamic urban scenes, Periodic Vibration Gaussian (PVG) [2] introduces temporal dynamics into Gaussian representations, unifying static and dynamic elements without manual annotations, while Street Gaussians [33] explicitly model foreground vehicles and backgrounds for efficient rendering. EmerNeRF [35] proposes a self-supervised spatial-temporal decomposition framework, capturing geometry, motion, and semantics without ground-truth annotations, and enhancing 3D perception tasks via lifted 2D foundation model features. DriveDreamer4D [43] bridges 4D reconstruction and world models, leveraging video generation priors to improve spatiotemporal coherence in novel trajectory views, outperforming prior Gaussian-based methods. STORM [36] adopts a feed-forward Transformer architecture to infer dynamic 3D Gaussians and velocities, enabling efficient large-scale outdoor scene reconstruction. FreeVS [27] introduces generative view synthesis for free trajectories, bypassing per-scene optimization through pseudo-image priors, while DrivingForward [24] achieves feed-forward reconstruction from sparse surround-view inputs via self-supervised pose and depth estimation. Despite these advancements, existing methods struggle to synthesize high-fidelity multi-modal sensor observations (*e.g.*, RGB videos, LiDAR point clouds, dense depth maps) in complex driving environments, particularly when rendering viewpoints that deviate significantly from recorded trajectories. To address these limitations, we propose a controllable multi-modal diffusion model to

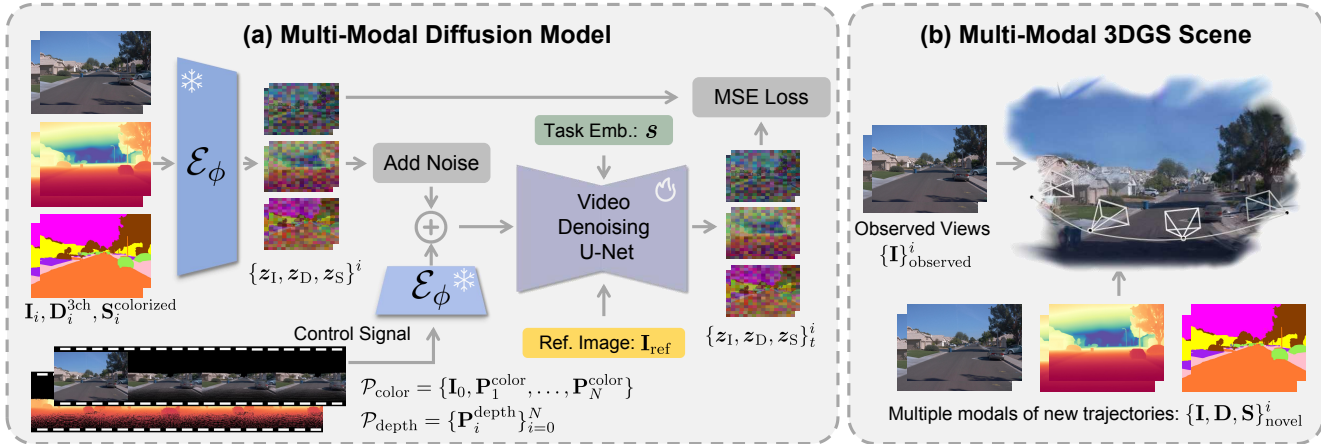


Figure 2. **Framework of MuDG.** (a) Training Phase of the Multi-modal Diffusion Model (MDM). Given a reference image and sparse conditions \mathcal{P}_{color} and \mathcal{P}_{depth} , we fine-tune the Video Diffusion Model to generate a color image I_i , a 3-channel depth map D_i^{3ch} and a colorized semantic map $S_i^{colorized}$ using multi-task embeddings s . (b) Pipeline of the Multi-modal 3DGS Scene. Using the dense output from the MDM module, we optimize a 3D Gaussian Splatting (3DGS) representation with better geometry-semantic consistency.

enable high-quality out-of-trajectory novel view synthesis.

2.2. Controllable Video Generation for Urban Scene

Recent advances in generative models have significantly propelled urban scene generation for autonomous driving, addressing challenges in 3D geometry control, multi-view consistency, and spatiotemporal dynamics [7, 8, 15–17, 29, 30, 44]. MagicDrive [7] introduces a framework for street-view synthesis with precise 3D controls (e.g., camera poses, road maps) via cross-view attention, enhancing 3D object detection and BEV segmentation. Extending this, MagicDrive3D [5] proposes a controllable 3D generation pipeline leveraging deformable Gaussian splatting to address unbounded street scenes, enabling high-fidelity any-view rendering. For dynamic scenarios, MagicDriveDiT [6] employs a DiT-based architecture with spatial-temporal latent conditioning to generate high-resolution, long-duration driving videos, while DreamDrive [20] combines video diffusion and hybrid Gaussian representations to synthesize 4D scenes with 3D-consistent dynamic video rendering. UniScene [16] presents an occupancy-centric approach to unify semantic, visual, and LiDAR data generation, reducing layout-to-data complexity through hierarchical learning strategies. DriveDreamer-2 [44] further enhances customization by integrating LLMs to generate user-defined driving videos with improved temporal coherence. Stag-1 [26] advances 4D simulation by decoupling spatial-temporal dynamics and leveraging point cloud reconstruction for photo-realistic, viewpoint-agnostic scene evolution. Recent concurrent works, such as StreetCrafter [34] and FreeVS [27], integrate generative diffusion models for controllable novel-view synthesis. However, these methods overlook the critical role of multi-modal data in achieving

high-quality reconstructions, resulting in suboptimal performance. In this work, we propose a novel controllable multi-modal diffusion model that simultaneously synthesizes high-quality RGB, depth, and semantic outputs for feed-forward novel-view synthesis, outperforming existing methods in terms of synthesis quality.

3. Method

In this section, we introduce **MuDG**, a framework that integrates a controllable **Multi-modal Diffusion** model with **Gaussian Splatting (GS)** for **Urban Scene Reconstruction**.

3.1. Overview

As illustrated in Fig. 2, our framework comprises two core components: a multi-modal diffusion model (MDM) and a Gaussian Splatting (GS) module. To enable feed-forward multi-modal synthesis, our MDM employs sparse RGB-depth conditions derived from fused LiDAR point clouds. We first separate dynamic objects from static backgrounds using tracking bounding boxes to create fused LiDAR point clouds. These point clouds are subsequently reprojected into sparse color and depth maps through perspective projection, forming the conditional inputs for our model.

As detailed in Sec. 3.2, MDM learns dense reconstructions (RGB, depth, and semantics) through joint training on sparse input pairs and ground-truth multi-modal data. By manipulating camera extrinsics, we generate novel conditional inputs through virtual viewpoint projection of the fused point cloud. This enables the diffusion model to synthesize reconstructed outputs ($I_i^{recon}, D_i^{recon}, S_i^{recon}$) for arbitrary perspectives through iterative denoising.

The GS module in Sec. 3.4 is then optimized using the reconstructed virtual viewpoints as supervision, minimizing

photometric and geometric discrepancies between rendered and reconstructed views. This optimization strategy ensures scene coherence under extreme camera motions while maintaining multi-modal alignment across viewpoints.

3.2. Controllable Multi-modal Diffusion Model

3.2.1. Preliminaries

Video diffusion models have recently achieved significant progress, primarily consisting of two key processes to learn the data distribution [1, 10]. In the forward diffusion process, at each time step $t \in \{1, \dots, T\}$, a gaussian noise $\epsilon \sim \mathcal{N}(0, I)$ is sampled and added to the initial latent representation \mathbf{x}_0 to obtain the noisy latent x_t . This process can be formally expressed as:

$$\mathbf{x}_t = \sqrt{\bar{\alpha}_t} \mathbf{x}_0 + \sqrt{1 - \bar{\alpha}_t} \epsilon, \quad (1)$$

where \mathbf{x}_t denotes the noisy latent at diffusion step t , and $\bar{\alpha}_t$ is the noise scheduling parameter.

In the reverse process, a denoising network \mathcal{F}_θ , parameterized by θ , is used to iteratively remove noise from \mathbf{x}_t and recover \mathbf{x}_{t-1} . During training, the network parameters θ are optimized by minimizing the following loss function:

$$\mathcal{L} = \mathbb{E}_{\mathbf{x}_0, \mathbf{c}, t \sim \mathcal{U}(T), \epsilon \sim \mathcal{N}(0, I)} \|\epsilon - \mathcal{F}_\theta(\mathbf{x}_t, \mathbf{c}, t)\|_2^2, \quad (2)$$

where \mathbf{c} represents optional conditioning information. At inference time, a noise sample \mathbf{x}_T is first drawn from a standard Gaussian distribution, and the denoising network \mathcal{F}_θ is applied iteratively to reconstruct the final output, such as an image or video frame.

3.2.2. Multi-modal Latent Encoding and Decoding

Following the common practice in video generation, we utilize a frozen pre-trained VAE [32] to encode RGB images, depth maps, and semantic maps into a unified latent space. Given three input modalities: RGB images $\mathbf{I}_i \in \mathbb{R}^{H \times W \times 3}$, single-channel depth maps $\mathbf{D}_i \in \mathbb{R}^{H \times W \times 1}$, and K-channel semantic maps $\mathbf{S}_i \in \mathbb{R}^{H \times W \times K}$, to satisfy the VAE’s input specifications, we convert the depth maps into pseudo-RGB images through channel replication, while transforming the semantic maps into RGB-compatible representations via colorization. The encoding process can be described as:

$$\mathbf{z}_I = \mathcal{E}(\mathbf{I}_i), \quad \mathbf{z}_D = \mathcal{E}(\mathbf{D}_i^{3\text{ch}}), \quad \mathbf{z}_S = \mathcal{E}(\mathbf{S}_i^{\text{colorized}}), \quad (3)$$

where \mathcal{E} denotes the VAE encoder, $\mathbf{D}_i^{3\text{ch}}$ is the 3-channel depth map, and $\mathbf{S}_i^{\text{colorized}}$ is the colorized semantic map.

During decoding, the VAE decoder reconstructs RGB, depth maps, and semantic maps from the latent space. For the depth map, we average the three channels of the decoder output to obtain the final single-channel depth map. For the semantic map, we revert the colorized output to the original labels via nearest-neighbor color matching. The decoding process can be described as follows:

$$\begin{aligned} \mathbf{I}_i^{\text{recon}} &= \mathcal{D}(\mathbf{z}_I), & \mathbf{D}_i^{\text{recon}} &= \frac{1}{3} \sum_{c=1}^3 \mathcal{D}(\mathbf{z}_D)_c, \\ \mathbf{S}_i^{\text{recon}} &= \arg \min_k \|\mathcal{D}(\mathbf{z}_S) - \text{Color}(k)\|_2, \end{aligned} \quad (4)$$

where \mathcal{D} denotes the VAE decoder, and $\text{Color}(k)$ represents the predefined color corresponding to the k -th semantic class.

3.2.3. Training Phase of MDM

As illustrated in Fig. 2(a), the training phase of MDM begins with random sampling of a known camera trajectory $\{\mathbf{C}_i\}_{i=0}^N$ paired with its dense observations $\mathcal{I} = \{\mathbf{I}_i\}_{i=0}^N$. Each view’s geometric and semantic information is represented through corresponding depth maps \mathcal{D} and semantic maps \mathcal{S} , denoted as $\mathcal{D} = \{\mathbf{D}_i\}_{i=0}^N$ and $\mathcal{S} = \{\mathbf{S}_i\}_{i=0}^N$, respectively. After fusion of LiDAR point clouds, we project point clouds into the image space using calibrated camera parameters, generating two sparse representations: sparse color images $\mathcal{P}_{\text{color}} = \{\mathbf{P}_i^{\text{color}}\}_{i=0}^N$ and sparse depth maps $\mathcal{P}_{\text{depth}} = \{\mathbf{P}_i^{\text{depth}}\}_{i=0}^N$. To establish spatial consistency, we designate the first frame as the reference view and substitute its corresponding sparse representation, forming our sparse conditional input as follows:

$$\mathcal{P}_{\text{color}} = \{\mathbf{I}_0, \mathbf{P}_1^{\text{color}}, \dots, \mathbf{P}_N^{\text{color}}\}. \quad (5)$$

We particularly emphasize that preserving the latent features of reference images in the conditional input queue is crucial for maintaining consistency between the generated results and the original scene. This design becomes essential as sparse LiDAR points inherently lack sufficient information to constrain the upper regions of the images, which necessitates the incorporation of the dense reference image to ensure control throughout the generation process.

Then, the dense images, depth maps, and semantic maps are encoded into latent representation with the VAE encoder $\mathbf{z}_I = \mathcal{E}(\mathcal{I})$, $\mathbf{z}_D = \mathcal{E}(\mathcal{D})$, and $\mathbf{z}_S = \mathcal{E}(\mathcal{S})$.

At each timestep t in training phase, we add noise to the sampled data $\mathbf{z} \in \{\mathbf{z}_I, \mathbf{z}_D, \mathbf{z}_S\}$, resulting in the noisy latent representations $\mathbf{z} \in \{\mathbf{z}_{I,t}, \mathbf{z}_{D,t}, \mathbf{z}_{S,t}\}$. Additionally, we encode the sparse color and depth inputs to obtain control signal: $\mathbf{y}_I = \mathcal{E}(\mathcal{P}_{\text{color}})$ and $\mathbf{y}_D = \mathcal{E}(\mathcal{P}_{\text{depth}})$. We then concatenate the noisy latent representations of each modality with the control signal as the input to the denoising diffusion network. The model is trained using a v-prediction objective, where the target \mathbf{v}_t is defined as:

$$\mathbf{v}_t = \alpha_t \epsilon_t - \sigma_t \mathbf{x}_t, \quad (6)$$

where $\epsilon_t \sim \mathcal{N}(\mathbf{0}, \mathbf{I})$ denotes the sampled gaussian noise, α_t and σ_t represent the time-dependent noise scheduling coefficients, and \mathbf{x}_t corresponds to the noisy input modality requiring denoising. The training objective is defined as:

$$\mathcal{L} = \mathbb{E}_{\mathbf{x}_t, \epsilon_t, \mathbf{s}} \|\mathcal{F}_\theta(\mathbf{x}_t, \mathbf{x}_{\text{ref}}, \mathbf{y}_I, \mathbf{y}_D, \mathbf{s}) - \mathbf{v}_t\|_2^2, \quad (7)$$

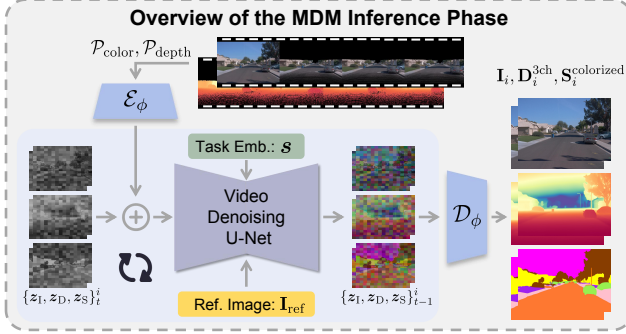


Figure 3. **Illustration of inference phase.** During inference, our multi-modal diffusion model takes a dense reference image and a sequence of condition images as inputs, generating the corresponding sequences of RGB, depth, and semantic maps.

y_I and y_D denote the sparse conditional inputs that guide the generation process, while x_{ref} provides the reference image for appearance consistency. The vector s represents the input modality that is denoised, with x_t indicating its noisy state in the diffusion time step t .

3.3. Inferring Phase of MDM

After MDM training, it can be directly applied as a generalized model to new scenarios without requiring per-scene optimization. Specifically, we first project the fused point clouds to novel viewpoints, yielding sparse color $\{I_{\text{sparse},i}\}_{i=1}^N$ and depth maps $\{D_{\text{sparse},i}\}_{i=0}^N$. We subsequently select adjacent observed images as reference views to form the input conditional as:

$$\mathcal{I}_{\text{cond}} = \{I_{\text{ref}}\} + \{I_{\text{sparse},i}\}_{i=1}^N, \quad \mathcal{D}_{\text{cond}} = \{D_{\text{sparse},i}\}_{i=0}^N. \quad (8)$$

As shown in Fig. 3, we initialize the generation process by sampling standard Gaussian noise z_T from a normal distribution. This noise vector is subsequently combined with encoded conditional inputs through channel-wise concatenation, where modality-specific guidance signals s are injected to steer different generation modalities. Consistent with the diffusion schedule used during training, we perform iterative denoising steps on the fused latent representation through our learned conditional diffusion process. The refined latent is finally decoded by the pre-trained VAE decoder to dense predictions in the pixel space, including color images, depth maps, and semantic maps.

3.4. Urban Scene View Synthesis

Current urban scene view synthesis methods tend to overfit training viewpoints, leading to significant artifacts when synthesizing novel views with significant perspective shifts (e.g., lane changes). This limitation arises from insufficient viewpoint diversity in training data, which severely constrains the generalization capability of 3DGS frameworks. To address this, we propose to leverage our multi-modal

diffusion model to generate novel view RGB images, depth maps, and semantic maps for providing rich supervisory for GS training and thereby improving the quality of novel view synthesis.

Specifically, we first generate novel camera trajectories, which is followed by generating corresponding novel view RGB images, depth maps, and semantic maps. To better utilize virtual viewpoints, during each training iteration, we select virtual viewpoints with a probability of θ . The overall optimization objective is defined as:

$$\mathcal{L}_{\text{input}} = \lambda_1 \mathcal{L}_1 + \lambda_{\text{ssim}} \mathcal{L}_{\text{ssim}} + \lambda_{\text{depth}} \mathcal{L}_{\text{depth}}, \quad (9)$$

$$\mathcal{L}_{\text{virtual}} = \lambda_{\text{v_color}} \mathcal{L}_{\text{lpiips}} + \lambda_{\text{v_depth}} \mathcal{L}_{\text{depth}} + \lambda_{\text{v_sem}} \mathcal{L}_{\text{sem}}, \quad (10)$$

where \mathcal{L}_1 , $\mathcal{L}_{\text{ssim}}$, $\mathcal{L}_{\text{lpiips}}$, and $\mathcal{L}_{\text{depth}}$ denote the L1, SSIM, LPIPS and depth loss, respectively. For virtual viewpoints, $\mathcal{L}_{\text{lpiips}}$, $\mathcal{L}_{\text{depth}}$, and \mathcal{L}_{sem} represent the LPIPS loss, depth loss, and Cross-Entropy loss, respectively.

4. Experiments

4.1. Implementation Details

Our multi-modal diffusion model (MDM) builds upon [32], following the original training configuration with v-objective. Specifically, we initialize MDM with the pre-trained weights of [32] while adapting its 8-channel input layers to accommodate our 12-channel inputs through weights replication and scaling. The training phase comprises two sequential stages: First, we train MDM with a resolution of 320×512 using a batch size of 8, learning rate of $1.0e-5$, and Adam optimizer for 20,000 iterations on $8 \times$ NVIDIA H20 GPUs, incorporating 20% random reference image dropout and a DDPM noise scheduler with 1,000 diffusion steps. Subsequently, we freeze the temporal layers and fine-tune the spatial components at a resolution of 576×1024 with reduced batch size 4 (same learning rate) for 8,000 iterations. For inference, we employ the DDIM [22] scheduler with 50-step sampling to balance efficiency and quality. The 3D Gaussian Splatting (3DGS) module adapts from [33], training each scene for 30,000 iterations on L20 GPUs with a 20% virtual viewpoint sampling probability to enhance geometric generalization.

4.2. Datasets

Our MDM is trained on the Open Waymo Dataset (WOD) [23] with 32 selected sequences. To generate sparse RGB and depth inputs, we aggregate lidars across the entire scene and project temporally fused point clouds onto each frame. For semantic map ground-truth, we employ the [31] to produce pseudo semantic maps for each frame. To obtain dense depth ground-truth, we first aggregate six consecutive LiDAR frames and project them into the current viewpoint, resulting in sparse LiDAR depth maps. Following established depth completion practices, these sparse maps are

Method	Shift 2m		Shift 3m		Shift 4m	
	FID ↓	FVD ↓	FID ↓	FVD ↓	FID ↓	FVD ↓
S ³ Gaussian [12]	169.08	2031.97	191.38	2543.47	206.99	2663.56
3DGS* [13]	101.63	1062.57	117.36	1379.68	135.10	1675.16
EmerNeRF [35]	73.58	645.90	93.09	983.94	110.94	1250.56
StreetGS [33]	69.79	<u>563.00</u>	87.71	898.05	100.05	1269.99
FreeVS [27]	92.08	652.09	95.91	784.74	117.68	<u>801.20</u>
Ours-R	50.02	671.24	49.42	<u>777.78</u>	56.52	770.39
Ours-S	<u>54.14</u>	509.34	<u>58.85</u>	659.27	<u>65.44</u>	808.85

Table 1. **Quantitative comparisons on novel view synthesis.** **Ours-R** denotes the outputs generated by our multi-modal diffusion model, while **Ours-S** integrates the results rendered from optimized 3D Gaussian Splatting Representation. 3DGS* denotes the results, excluding failure cases. Our method demonstrates superior quality even under large viewpoint displacements, such as ± 4 -meter lateral shifts. Furthermore, **Ours-R** exhibits exceptional robustness to variations in camera pose. (**Bold** figures indicate the best and underlined figures indicate the second best)

first densified using [18], then geometrically aligned with the original LiDAR measurements through least-squares optimization to ensure consistency.

4.3. Experimental Results

4.3.1. Multi-model Results

This paper introduces a novel framework for multi-modal novel view synthesis in street scenes under extreme viewpoint changes. As shown in Fig. 4, our MDM enables feed-forward novel view synthesis from sparse depth and color inputs while generating consistent RGB, depth, and semantic maps. This view-aligned multi-modal generation capability directly supports autonomous driving applications through synthetic data generation and enhanced 3D reconstruction.

As shown in Fig. 6, our model’s controllability allows precise editing, including background replacement, lane changes, and object removal. It also generates aligned multi-modal outputs (RGB, depth, semantics) that maintain consistency during editing.

4.3.2. Benchmark Evaluation

In this section, we compare our approach with state-of-the-art street view synthesis methods, as quantitatively presented in Tab. 1. Here, Ours-R represents the outputs of MDM, while Ours-S denotes the MuDG approach, which integrates MDM with the 3DGS module. Since ground truth is unavailable for novel view synthesis outputs in the lane-shifting setting, we evaluate rendering quality using Fréchet Inception Distance (FID) [9] and Fréchet Video Distance (FVD) [28]. As shown in Tab. 1, our method outperforms existing methods by a large margin and achieves state-of-the-art performance. Notably, Ours-R demonstrates greater stability under extreme viewpoint shifts ($-4m$ lateral) than Ours-S. This is due to Ours-S’s susceptibility to artifacts at scene boundaries, whereas Ours-R maintains photorealistic

Setting	Ref. Img	Sparse Cond.	SSIM ↑	PSNR ↑	LPIPS ↓	FID ↓
(a)	✓	-	0.539	19.09	0.325	31.33
(b)	-	✓	0.631	22.01	0.254	25.17
(c)	✓	✓	<u>0.642</u>	<u>22.48</u>	<u>0.238</u>	<u>23.66</u>
Full Model	✓	✓	0.643	22.49	0.237	23.29

Table 2. **Ablation Studies on Control Signal.** Module (a) utilizes only reference images as control signal, while module (b) employs sparse conditions. Module (c) simply concatenate both information, whereas our full model injects the reference image only into the first frame of the sparse condition while maintaining other sparse conditions as spatiotemporal control signals. The results underscore the efficiency and quality of our designed model.

Setting	I _v	D _v	S _v	SSIM ↑	PSNR ↑	LPIPS ↓	FID ↓	FVD ↓
(a)	-	-	-	0.916	31.96	0.085	39.62	283.05
(b)	✓	-	-	<u>0.910</u>	31.46	0.091	32.20	217.17
(c)	✓	✓	-	0.910	31.54	0.090	<u>32.00</u>	216.14
(d)	✓	-	✓	0.910	31.51	0.091	32.17	<u>214.22</u>
Full Model	✓	✓	✓	0.910	<u>31.60</u>	<u>0.090</u>	31.94	209.79

Table 3. **Ablation on Multi-modal Supervision for 3DGS.** The results demonstrate the significance of multi-modal supervision for 3DGS reconstruction. All multi-modal supervisions contribute to the 3DGS representation, particularly in dynamic urban scenes.

consistency even in these challenging regions. Here, we observe that the 3DGS module fails in two dynamic scenes due to the rare initialization of Gaussian points and the metrics for 3DGS* are calculated based on the remaining scenes.

We compare the visualization results of 3DGS [14], S³Gaussian [12], and StreetGaussian [33] with our model in Fig. 5, where our method generates higher-quality novel views under shifted viewpoints. Notably, Ours-R demonstrates robust generalization with sparse input conditions, producing photorealistic lane-shift renderings without per-scene optimization. Meanwhile, Ours-S enhances overall consistency and geometric detail by integrating the 3D Gaussian Splatting model. This hybrid approach effectively balances the fidelity of diffusion-based generation with the explicit representation of 3D scenes, surpassing baseline methods in both visual realism and structural preservation under extreme viewpoint variations.

Fig. 7 visualizes the depth maps in the novel viewpoints, demonstrating that our method, which combines multi-modal diffusion and 3DGS maintained the better geometric quality under significant viewpoint offsets.

4.3.3. Ablation Study

In this section, we conduct the ablation study to analyze the effectiveness of each module of MuDG.

Ablation on Control Signal. As shown in Tab. 2, we evaluate our diffusion model’s novel view synthesis capability under different control signals. The base model using only reference images (Tab. 2 (a)) performs the weakest (SSIM 0.54, FID 31.33), highlighting the limitations of static single-view inputs. Using only sparse conditions (Tab. 2 (b)) improves SSIM by 17% and reduces FID by

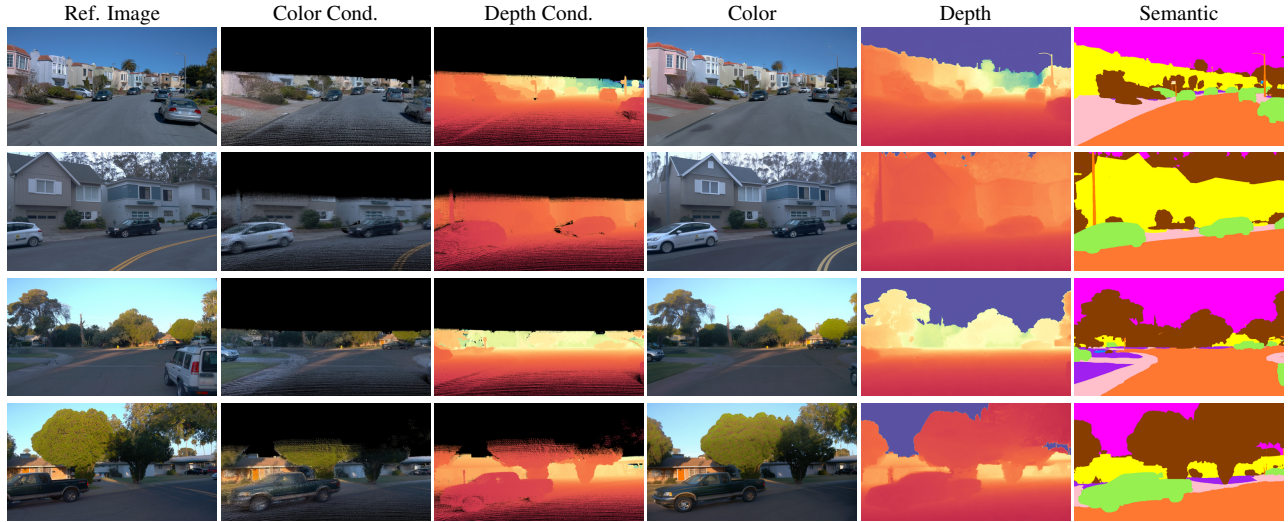


Figure 4. **Visualization of multi-modal results.** Given the reference image and sparse conditions, we present the visualized multi-modal novel-view synthesis results (color, depth, and semantic map). The depth maps are visualized in the range of $[0, 100m]$. The controllable and photorealistic results highlight the robust multi-modal synthesis capabilities of our approach, even under extreme viewpoint variations.

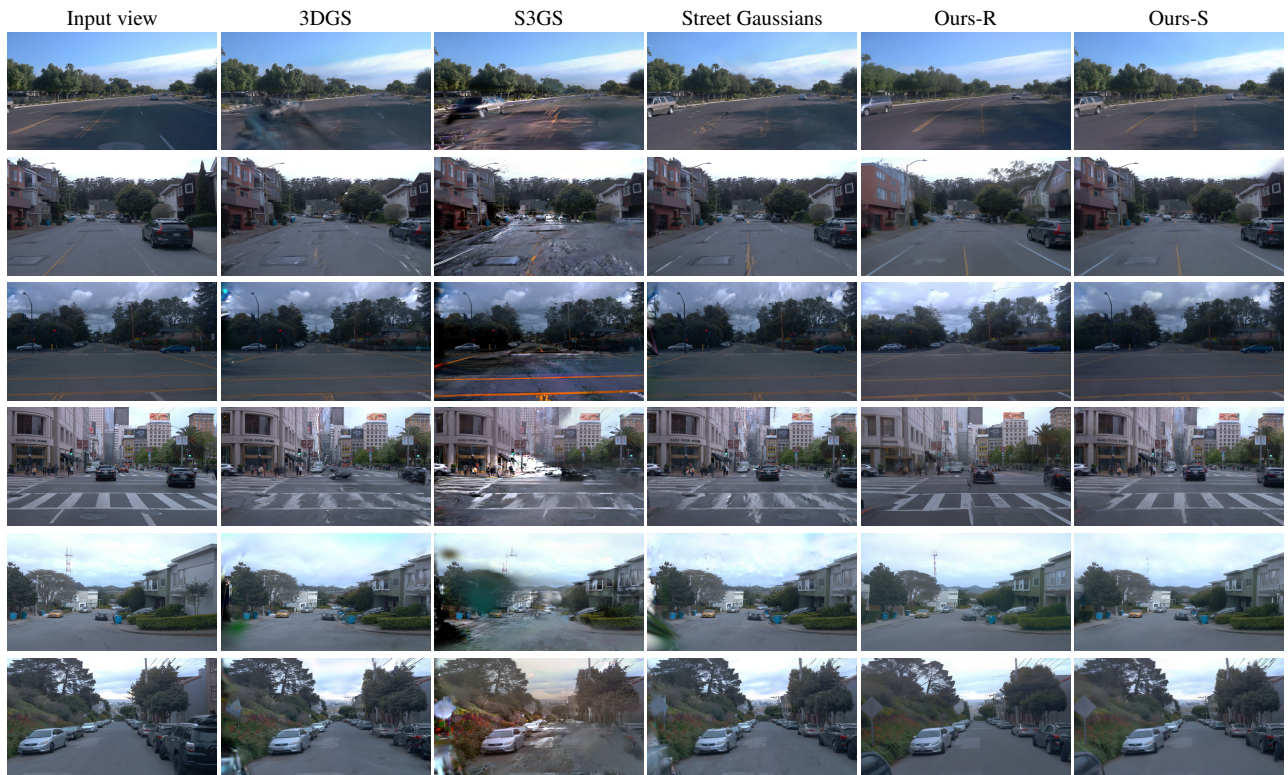


Figure 5. **Qualitative Comparison of Novel View Synthesis on the Open Waymo Dataset.** We evaluate novel view synthesis using a 2-meter leftward camera offset. **Ours-R** refers to the outputs generated by our multi-modal diffusion model, which relies exclusively on sparse conditional inputs (color and depth). In contrast, **Ours-S** represents the results of the 3D Gaussian Splatting (3DGS) model, which is trained in a supervised manner using the outputs from Ours-R module as training signals. Our approach achieves photorealistic consistency and demonstrates superior geometric stability under significant viewpoint changes, outperforming existing baseline methods.

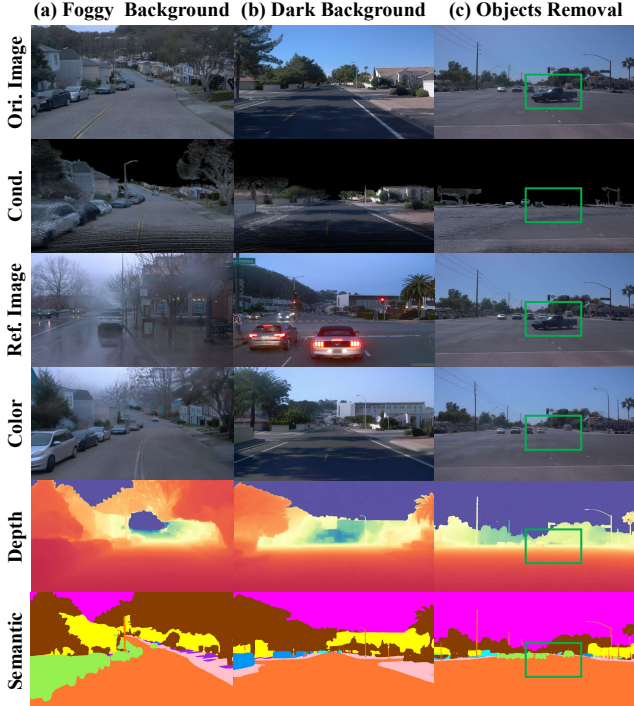


Figure 6. **Visualization of editing results.** The figure demonstrates the ability of MDM to edit the background, such as transforming it into a foggy or dark setting, and to remove objects. MDM can effectively modify the target area based on the reference image while maintaining consistency with original images.

19.6%, demonstrating their effectiveness in encoding camera poses and motion trajectories. However, sparse conditions alone remains insufficient for consistent generation in unobserved regions. Combining reference images with sparse conditions (Tab. 2 (c)) leads to moderate improvements: PSNR increases from 22.01 to 22.48, while LPIPS decreases by 6%, indicating the complementary nature of static and dynamic cues. To further enhance performance, our optimized architecture strategically places the reference image as the first sparse input frame (Full Model), achieving superior metrics while reducing channel capacity by half (from 8 to 4 channels). This design not only preserves spatiotemporal consistency but also replace brute-force channel expansion via concatenation and mitigating feature misalignment. Additionally, our streamlined architecture reduces network parameters, improving efficiency without compromising synthesis quality.

Ablation on Multi-modal Supervision for 3DGS. The Tab. 3 quantifies the impact of virtual viewpoint multi-modal results (dense color I_v , depth D_v , and semantic maps S_v) generated from MDM serving as supervision on 3DGS reconstruction. Integrating multi-modal virtual views significantly improves the quality of the novel view synthesis. Specifically, incorporating virtual view color information reduces FID by 18.7% and improves FVD by 23.3%,

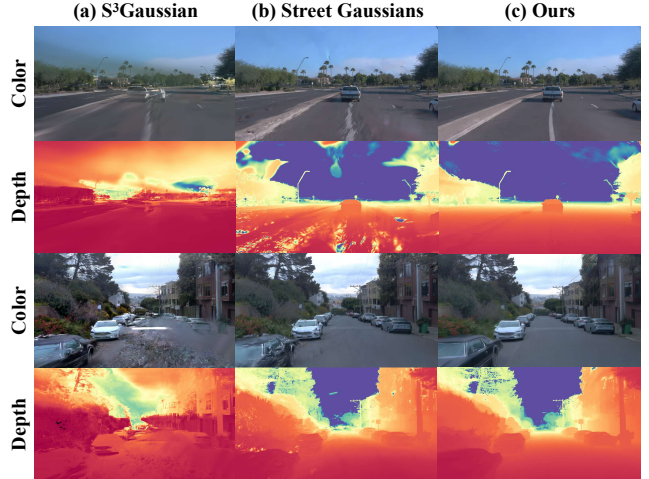


Figure 7. **The qualitative comparisons of depth rendering.** The results demonstrate the high geometric quality of our method, achieving superior depth rendering outcomes.

indicating that augmented virtual views effectively bridge the distribution gap between synthetic and real data while improving temporal coherence in video sequences. Additionally, depth information from virtual views enhances geometric consistency, while semantic information strengthens scene structural coherence. Although virtual views introduce minor pixel-level deviations (SSIM / PSNR drop $\sim 0.5\%$), multimodal fusion significantly improves scene plausibility and temporal stability, as reflected in a progressive 26% FVD reduction. These findings highlight the critical role of cross-view alignment in dynamic scene modeling, particularly for urban scene view synthesis.

5. Conclusion

We present MuDG, an innovative framework that synergizes controllable multi-modal diffusion models with 3D Gaussian Splatting for robust urban scene reconstruction and view synthesis. By conditioning our diffusion model on aggregated LiDAR data and multi-modal priors, our proposed MDM is able to synthesize multi-modal results under novel viewpoints with no need of per-scene optimization. The synthesized dense RGB, depth, and semantic outputs not only enable feed-forward novel view synthesis but also significantly improve 3DGS training through enriched supervision signals. Extensive experiments validate that our framework achieves state-of-the-art performance in urban scene reconstruction and novel view synthesis.

Limitations and Future Work. Our MDM is built on a denoising diffusion UNet, which entails substantial time costs for both training and inference. Thus, accelerating the model is a key area for improvement. Additionally, our training process relies on pre-processed pseudo ground truths (depth and semantic maps), further contributing to the overall time

expense. Optimizing the generation process of pseudo GTs will be another crucial focus for future enhancements.

References

- [1] Andreas Blattmann, Tim Dockhorn, Sumith Kulal, Daniel Mendelevitch, Maciej Kilian, Dominik Lorenz, Yam Levi, Zion English, Vikram Voleti, Adam Letts, et al. Stable video diffusion: Scaling latent video diffusion models to large datasets. *arXiv preprint arXiv:2311.15127*, 2023. 4
- [2] Yurui Chen, Chun Gu, Junzhe Jiang, Xiatian Zhu, and Li Zhang. Periodic vibration gaussian: Dynamic urban scene reconstruction and real-time rendering. *arXiv preprint arXiv:2311.18561*, 2023. 1, 2
- [3] Sara Fridovich-Keil, Alex Yu, Matthew Tancik, Qinlong Chen, Benjamin Recht, and Angjoo Kanazawa. Plenoxels: Radiance fields without neural networks. In *Proceedings of the IEEE/CVF conference on computer vision and pattern recognition*, pages 5501–5510, 2022. 1, 2
- [4] Xiao Fu, Wei Yin, Mu Hu, Kaixuan Wang, Yuexin Ma, Ping Tan, Shaojie Shen, Dahua Lin, and Xiaoxiao Long. Geowizard: Unleashing the diffusion priors for 3d geometry estimation from a single image. In *European Conference on Computer Vision*, pages 241–258. Springer, 2024. 1
- [5] Ruiyuan Gao, Kai Chen, Zhihao Li, Lanqing Hong, Zhenguo Li, and Qiang Xu. Magicdrive3d: Controllable 3d generation for any-view rendering in street scenes. *arXiv preprint arXiv:2405.14475*, 2024. 3
- [6] Ruiyuan Gao, Kai Chen, Bo Xiao, Lanqing Hong, Zhenguo Li, and Qiang Xu. Magicdrivedit: High-resolution long video generation for autonomous driving with adaptive control. *arXiv preprint arXiv:2411.13807*, 2024. 3
- [7] Ruiyuan Gao, Kai Chen, Enze Xie, Lanqing Hong, Zhenguo Li, Dit-Yan Yeung, and Qiang Xu. Magicdrive: Street view generation with diverse 3d geometry control. In *ICLR*, 2024. 2, 3
- [8] Shenyan Gao, Jiazhi Yang, Li Chen, Kashyap Chitta, Yihang Qiu, Andreas Geiger, Jun Zhang, and Hongyang Li. Vista: A generalizable driving world model with high fidelity and versatile controllability. *arXiv preprint arXiv:2405.17398*, 2024. 3
- [9] Martin Heusel, Hubert Ramsauer, Thomas Unterthiner, Bernhard Nessler, and Sepp Hochreiter. Gans trained by a two time-scale update rule converge to a local nash equilibrium. *Advances in neural information processing systems*, 30, 2017. 6
- [10] Jonathan Ho, Ajay Jain, and Pieter Abbeel. Denoising diffusion probabilistic models. *Advances in neural information processing systems*, 33:6840–6851, 2020. 4
- [11] Binbin Huang, Zehao Yu, Anpei Chen, Andreas Geiger, and Shenghua Gao. 2d gaussian splatting for geometrically accurate radiance fields. In *ACM SIGGRAPH 2024 conference papers*, pages 1–11, 2024. 1, 2
- [12] Nan Huang, Xiaobao Wei, Wenzhao Zheng, Pengju An, Ming Lu, Wei Zhan, Masayoshi Tomizuka, Kurt Keutzer, and Shanghang Zhang. S3gaussian: Self-supervised street gaussians for autonomous driving. *arXiv preprint arXiv:2405.20323*, 2024. 1, 2, 6
- [13] Bernhard Kerbl, Georgios Kopanas, Thomas Leimkühler, and George Drettakis. 3d gaussian splatting for real-time radiance field rendering. *ACM Trans. Graph.*, 42(4):139–1, 2023. 2, 6
- [14] Bernhard Kerbl, Georgios Kopanas, Thomas Leimkühler, and George Drettakis. 3d gaussian splatting for real-time radiance field rendering. *ACM Trans. Graph.*, 2023. 1, 2, 6
- [15] Bohan Li, Jiajun Deng, Wenyao Zhang, Zhujin Liang, Dalong Du, Xin Jin, and Wenjun Zeng. Hierarchical temporal context learning for camera-based semantic scene completion. In *European Conference on Computer Vision*, pages 131–148. Springer, 2024. 3
- [16] Bohan Li, Jiazhe Guo, Hongsi Liu, Yingshuang Zou, Yikang Ding, Xiwu Chen, Hu Zhu, Feiyang Tan, Chi Zhang, Tiancai Wang, et al. Uniscene: Unified occupancy-centric driving scene generation. *arXiv preprint arXiv:2412.05435*, 2024. 2, 3
- [17] Bohan Li, Yasheng Sun, Jingxin Dong, Zheng Zhu, Jiming Liu, Xin Jin, and Wenjun Zeng. One at a time: Progressive multi-step volumetric probability learning for reliable 3d scene perception. In *Proceedings of the AAAI Conference on Artificial Intelligence*, pages 3028–3036, 2024. 3
- [18] Zhiheng Liu, Ka Leong Cheng, Qiuyu Wang, Shuzhe Wang, Hao Ouyang, Bin Tan, Kai Zhu, Yujun Shen, Qifeng Chen, and Ping Luo. Depthlab: From partial to complete. *arXiv preprint arXiv:2412.18153*, 2024. 6
- [19] Xiaoxiao Long, Yuan-Chen Guo, Cheng Lin, Yuan Liu, Zhiyang Dou, Lingjie Liu, Yuexin Ma, Song-Hai Zhang, Marc Habermann, Christian Theobalt, et al. Wonder3d: Single image to 3d using cross-domain diffusion. In *Proceedings of the IEEE/CVF conference on computer vision and pattern recognition*, pages 9970–9980, 2024. 1
- [20] Jiageng Mao, Boyi Li, Boris Ivanovic, Yuxiao Chen, Yan Wang, Yurong You, Chaowei Xiao, Danfei Xu, Marco Pavone, and Yue Wang. Dreamdrive: Generative 4d scene modeling from street view images. *arXiv preprint arXiv:2501.00601*, 2024. 3
- [21] Ben Mildenhall, Pratul P Srinivasan, Matthew Tancik, Jonathan T Barron, Ravi Ramamoorthi, and Ren Ng. Nerf: Representing scenes as neural radiance fields for view synthesis. *Communications of the ACM*, 65(1):99–106, 2021. 1, 2
- [22] Jiaming Song, Chenlin Meng, and Stefano Ermon. Denoising diffusion implicit models. *arXiv preprint arXiv:2010.02502*, 2020. 5
- [23] Pei Sun, Henrik Kretzschmar, Xerxes Dotiwalla, Aurelien Chouard, Vijaysai Patnaik, Paul Tsui, James Guo, Yin Zhou, Yuning Chai, Benjamin Caine, et al. Scalability in perception for autonomous driving: Waymo open dataset. In *Proceedings of the IEEE/CVF conference on computer vision and pattern recognition*, pages 2446–2454, 2020. 2, 5
- [24] Qijian Tian, Xin Tan, Yuan Xie, and Lizhuang Ma. Drivingforward: Feed-forward 3d gaussian splatting for driving scene reconstruction from flexible surround-view input. *arXiv preprint arXiv:2409.12753*, 2024. 2

- [25] Adam Tonderski, Carl Lindström, Georg Hess, William Ljungbergh, Lennart Svensson, and Christoffer Petersson. Neurad: Neural rendering for autonomous driving. In *Proceedings of the IEEE/CVF Conference on Computer Vision and Pattern Recognition*, pages 14895–14904, 2024. 2
- [26] Lening Wang, Wenzhao Zheng, Dalong Du, Yunpeng Zhang, Yilong Ren, Han Jiang, Zhiyong Cui, Haiyang Yu, Jie Zhou, Jiwen Lu, et al. Stag-1: Towards realistic 4d driving simulation with video generation model. *arXiv preprint arXiv:2412.05280*, 2024. 3
- [27] Qitai Wang, Lue Fan, Yuqi Wang, Yuntao Chen, and Zhaoxiang Zhang. Freevs: Generative view synthesis on free driving trajectory. *arXiv preprint arXiv:2410.18079*, 2024. 2, 3, 6
- [28] Ting-Chun Wang, Ming-Yu Liu, Jun-Yan Zhu, Guilin Liu, Andrew Tao, Jan Kautz, and Bryan Catanzaro. Video-to-video synthesis. *arXiv preprint arXiv:1808.06601*, 2018. 6
- [29] Xiaofeng Wang, Zheng Zhu, Guan Huang, Xinze Chen, and Jiwen Lu. Drivedreamer: Towards real-world-driven world models for autonomous driving. *ECCV*, 2024. 2, 3
- [30] Yuqi Wang, Jiawei He, Lue Fan, Hongxin Li, Yuntao Chen, and Zhaoxiang Zhang. Driving into the future: Multiview visual forecasting and planning with world model for autonomous driving. In *CVPR*, 2024. 2, 3
- [31] Enze Xie, Wenhai Wang, Zhiding Yu, Anima Anandkumar, Jose M Alvarez, and Ping Luo. Segformer: Simple and efficient design for semantic segmentation with transformers. *Advances in neural information processing systems*, 34: 12077–12090, 2021. 5
- [32] Jinbo Xing, Menghan Xia, Yong Zhang, Haoxin Chen, Wangbo Yu, Hanyuan Liu, Gongye Liu, Xintao Wang, Ying Shan, and Tien-Tsin Wong. Dynamicrafter: Animating open-domain images with video diffusion priors. In *European Conference on Computer Vision*, pages 399–417. Springer, 2024. 4, 5
- [33] Yunzhi Yan, Haotong Lin, Chenxu Zhou, Weijie Wang, Haiyang Sun, Kun Zhan, Xianpeng Lang, Xiaowei Zhou, and Sida Peng. Street gaussians: Modeling dynamic urban scenes with gaussian splatting. In *European Conference on Computer Vision*, pages 156–173. Springer, 2024. 1, 2, 5, 6
- [34] Yunzhi Yan, Zhen Xu, Haotong Lin, Haijin Jin, Haoyu Guo, Yida Wang, Kun Zhan, Xianpeng Lang, Hujun Bao, Xiaowei Zhou, et al. Streetrafter: Street view synthesis with controllable video diffusion models. *arXiv preprint arXiv:2412.13188*, 2024. 3
- [35] Jiawei Yang, Boris Ivanovic, Or Litany, Xinshuo Weng, Seung Wook Kim, Boyi Li, Tong Che, Danfei Xu, Sanja Fidler, Marco Pavone, et al. Emernerf: Emergent spatial-temporal scene decomposition via self-supervision. *arXiv preprint arXiv:2311.02077*, 2023. 1, 2, 6
- [36] Jiawei Yang, Jiahui Huang, Yuxiao Chen, Yan Wang, Boyi Li, Yurong You, Apoorva Sharma, Maximilian Igl, Peter Karkus, Danfei Xu, et al. Storm: Spatio-temporal reconstruction model for large-scale outdoor scenes. *arXiv preprint arXiv:2501.00602*, 2024. 2
- [37] Ze Yang, Yun Chen, Jingkan Wang, Sivabalan Manivasagam, Wei-Chiu Ma, Anqi Joyce Yang, and Raquel Urtasun. Unisim: A neural closed-loop sensor simulator. In *CVPR*, 2023. 1, 2
- [38] Ze Yang, Yun Chen, Jingkan Wang, Sivabalan Manivasagam, Wei-Chiu Ma, Anqi Joyce Yang, and Raquel Urtasun. Unisim: A neural closed-loop sensor simulator. In *Proceedings of the IEEE/CVF Conference on Computer Vision and Pattern Recognition*, pages 1389–1399, 2023. 1
- [39] Wangbo Yu, Jinbo Xing, Li Yuan, Wenbo Hu, Xiaoyu Li, Zhipeng Huang, Xiangjun Gao, Tien-Tsin Wong, Ying Shan, and Yonghong Tian. Viewrafter: Taming video diffusion models for high-fidelity novel view synthesis. *arXiv preprint arXiv:2409.02048*, 2024. 2
- [40] Zehao Yu, Anpei Chen, Binbin Huang, Torsten Sattler, and Andreas Geiger. Mip-splatting: Alias-free 3d gaussian splatting. In *Proceedings of the IEEE/CVF conference on computer vision and pattern recognition*, pages 19447–19456, 2024. 1, 2
- [41] Chuanrui Zhang, Yingshuang Zou, Zhuoling Li, Minmin Yi, and Haoqian Wang. Transplat: Generalizable 3d gaussian splatting from sparse multi-view images with transformers. *arXiv preprint arXiv:2408.13770*, 2024. 1
- [42] Kai Zhang, Gernot Riegler, Noah Snavely, and Vladlen Koltun. Nerf++: Analyzing and improving neural radiance fields. *arXiv preprint arXiv:2010.07492*, 2020. 1, 2
- [43] Guosheng Zhao, Chaojun Ni, Xiaofeng Wang, Zheng Zhu, Xueyang Zhang, Yida Wang, Guan Huang, Xinze Chen, Boyuan Wang, Youyi Zhang, et al. Drivedreamer4d: World models are effective data machines for 4d driving scene representation. *arXiv preprint arXiv:2410.13571*, 2024. 2
- [44] Guosheng Zhao, Xiaofeng Wang, Zheng Zhu, Xinze Chen, Guan Huang, Xiaoyi Bao, and Xingang Wang. Drivedreamer-2: Llm-enhanced world models for diverse driving video generation. *arXiv preprint arXiv:2403.06845*, 2024. 2, 3
- [45] Hongyu Zhou, Jiahao Shao, Lu Xu, Dongfeng Bai, Weichao Qiu, Bingbing Liu, Yue Wang, Andreas Geiger, and Yiyi Liao. Hugs: Holistic urban 3d scene understanding via gaussian splatting. In *Proceedings of the IEEE/CVF Conference on Computer Vision and Pattern Recognition*, pages 21336–21345, 2024. 1, 2
- [46] Xiaoyu Zhou, Zhiwei Lin, Xiaojun Shan, Yongtao Wang, Deqing Sun, and Ming-Hsuan Yang. Drivinggaussian: Composite gaussian splatting for surrounding dynamic autonomous driving scenes. In *Proceedings of the IEEE/CVF conference on computer vision and pattern recognition*, pages 21634–21643, 2024. 1, 2
- [47] Yingshuang Zou, Yikang Ding, Xi Qiu, Haoqian Wang, and Haotian Zhang. M2depth: Self-supervised two-frame multi-camera metric depth estimation. In *European Conference on Computer Vision*, pages 269–285. Springer, 2024. 1